A&A 586, A62 (2016)
DOI: 10.1051/0004-6361/201527018

Astronomy & Astrophysics

A map of D/H on Mars in the thermal infrared using EXES aboard SOFIA

T. Encrenaz[1], C. DeWitt[2], M. J. Richter[2], T. K. Greathouse[3], T. Fouchet[1], F. Montmessin[4], F. Lefèvre[4], F. Forget[5], B. Bézard[1], S. K. Atreya[6], M. Case[2], and N. Ryde[7]

[1] LESIA, Observatoire de Paris, CNRS, PSL, UPMC, UPD, 92195 Meudon, France
e-mail: therese.encrenaz@obspm.fr
[2] Dept. of Physics, University of California Davis, CA 95616, USA
[3] SwRI, Div. 15, San Antonio, TX 78228, USA
[4] LATMOS, IPSL, 75252 Paris Cedex 05, France
[5] LMD, IPSL, 75252 Paris Cedex 05, France
[6] Dept. of Atmospheric, Oceanic & Space Sciences, University of Michigan, Ann Arbor, MI 48109-2143, USA
[7] Department of Astronomy and Theoretical Physics, Lund Observatory, Lund University, Box 43, 221 00 Lund, Sweden

Received 21 July 2015 / Accepted 30 November 2015

ABSTRACT

On a planetary scale, the D/H ratio on Mars is a key diagnostic for understanding the past history of water on the planet; locally, it can help to constrain the sources and sinks of water vapor through the monitoring of condensation and sublimation processes. To obtain simultaneous measurements of H_2O and HDO lines, we have used the Echelle Cross Echelle Spectrograph (EXES) instrument aboard the Stratospheric Observatory for Infrared Astronomy (SOFIA) facility to map the abundances of these two species over the Martian disk. High-resolution spectra ($R = 6 \times 10^4$) were recorded in the 1383−1390 cm^{-1} range (7.2 μm) on April 08, 2014. Mars was very close to opposition and near northern summer solstice (Ls = 113°). Maps of the H_2O and HDO mixing ratios were retrieved from the line depth ratios of weak H_2O and HDO transitions divided by a weak CO_2 line. As expected for this season, the H_2O and HDO maps show a distinct enhancement toward polar regions, and their mixing ratios are consistent with previous measurements and with predictions by the global climate models, except at the north pole where the EXES values are weaker. We derive a disk-integrated D/H ratio of 6.8 (+1.6, −1.0) $\times 10^{-4}$. It is higher than the value in Earth's oceans by a factor 4.4 (+1.0, −0.6). The D/H map also shows an enhancement from southern to northern latitudes, with values ranging from about 3.5 times to 6.0 times the VSMOW (Vienna standard mean ocean water) value. The D/H distribution shows a depletion over the Tharsis mountains and is consistent with observed latitudinal variations. The variations in D/H with latitude and altitude agree with the models and with the isotope fractionation expected from condensation and sublimation processes.

Key words. planets and satellites: atmospheres – planets and satellites: composition – planets and satellites: terrestrial planets – infrared: planetary systems

1. Introduction

Measuring the D/H ratio in the Martian atmosphere is important for two reasons. On a global scale, the disk-integrated estimate of this ratio, compared with its value in past measurements in the most ancient SNC meteorites and/or in clays at the Martian surface is a tracer of the abundance of the early content of water on Mars (Greenwood et al. 2008; Mahaffy et al. 2015). Indeed, the main mechanism responsible for the deuterium enrichment in the Martian atmosphere is expected to be fractionation through differential escape rates, the HDO molecule being heavier than H_2O and confined at low altitude by condensation (Bertaux & Montmessin 2001).

The HDO molecule was first detected on Mars by Owen et al. (1988) who from near-infrared ground-based observations inferred a disk-averaged ratio for D/H in water enriched by a factor of 6+/−3 relative to the value in Earth's oceans (the VSMOW is 1.556×10^{-4}). The second measurement of D/H in Mars water (from the *Kuiper* Airborne Observatory) sampled CO_2, HDO, and H_2O simultaneously in the 2.7 μm region and found that D/H was enriched by a factor of 5.2+/−0.2 relative to the VSMOW (Bjoraker et al. 1989). Again in the near-infrared range, Krasnopolsky et al. (1997) inferred a D/H enrichment of 5.2+/−2.0 times the VSMOW. Encrenaz et al. (1991, 2001) detected HDO in the millimeter range and derived a D/H ratio of six (+6, −3) times the VSMOW in the northern hemisphere at northern summer solstice.

Attempts to map D/H on Mars as a function of location, altitude, and season were reported by Mumma et al. (2003) using data from 1997 through 2000 and by Novak et al. (2011) using data obtained from 2008 to 2010. They were completed by Villanueva et al. (2015), who mapped D/H over a broad latitude range between the northern spring equinox and the northern summer solstice. From data obtained between 2007 and 2015, Krasnopolsky (2015) also recorded latitudinal variations of D/H for different times around northern spring.

As discussed by Owen et al. (1988) and Owen (1992), a deuterium enrichment of 5 × VSMOW or greater, compared to the terrestrial value, requires the destruction and escape of most of the water originally present on the Martian surface. This process, however, would imply that the early hydrogen escape was much faster than observed today (McElroy et al. 1977). Another open question is related to the very large amount of liquid water apparently required to account for the erosional features observed on

the surface of Mars. These results have been discussed by several authors (Carr 1986, 1990, 1996; Jakosky 1990; Krasnopolsky et al. 1997; Lasue et al. 2013; Wordsworth et al. 2015).

In their recent analysis, Villanueva et al. (2015) estimate the water amount contained in the initial reservoir M_P using the following equation:

$$M_P/M_C = [I_C/I_P] \exp[1/(1-f)]$$

where M_C is the current water reservoir, I_P and I_C are the initial and current isotopic ratios, respectively, and f is the fractionation escape rate. Using $f = 0.02$ from Lyα measurements by Krasnopolsky et al. (1998), $I_C = 8$ and $I_P = 1.275$ (using the SNC meteorite analysis of Usui et al. 2012), the authors derive $[I_P/I_C] = 6.4$. Using for M_C, a value of 21 m GEL (global equivalent layer) inferred from the polar layered deposits by Zuber et al. (1998) and Plaut et al. (2007), they derive an initial water reservoir of 137 m GEL. This result is consistent with the idea of an ancient northern ocean covering about 20% of the Martian surface, as also suggested by the MARSIS radar observations of Mars Express (Mouginot et al. 2012).

Another estimate of the lost water is derived by Krasnopolsky (2015), who infers a value of 80 m GEL from an update of earlier analyses (Krasnopolsky & Feldman 2001; Krasnopolsky 2002). Krasnopolsky (2015) also suggests that, because the liquid water ocean may be insufficient to drive hydrodynamical escape, another more efficient hydrodynamical mechanism could be the escape of hydrogen released in the reaction of water with iron just after the planet's accretion. Using a fractionation factor of 0.8 in this case (Zahnle et al. 1990), an initial water abundance of 1200 m is inferred by Krasnopolsky (2015), confirming an earlier analysis by Krasnopolsky & Feldman (2001).

An important result is the measurement by the SAM (sample analysis at Mars) experiment aboard the Curiosity rover on ancient clays, aged about 3 Ga. The inferred D/H value, 3.0+/−0.2 times the VSMOW (Mahaffy et al. 2015), is intermediate between the primordial and present values, which suggests a continuous hydrogen escape over the history of the planet. However, the analysis of ancient SNC meteorites (in particular D/H = 4 VSMOW in ALH84001, aged over 4 Gy; Greenberg et al. 2008) instead suggested an early massive outgassing (Boctor et al. 2003; Greenwood et al. 2008). Thus, the history of water outgassing on Mars is still an open question.

On a local scale, the measurement of D/H on Mars as a function of altitude, location, and season can provide important constraints on the mechanisms responsible for the sources and sinks of water vapor on the Martian surface. The main mechanism is the so-called vapor pressure isotopic effect (VPIE), a fractionation mechanism associated with condensation/sublimation processes. At thermochemical equilibrium, the HDO/H_2O ratio in ice, as compared with the gas phase, decreases as temperature increases (Merlivat & Leaf 1967). At condensation, D/H is thus enriched in the ice phase, as compared with the gas phase. The D/H ratio in water vapor is expected to be maximum at the north pole at northern summer solstice, following the massive outgassing of the northern water ice cap. In the same way, this ratio is expected to increase with the water vapor content and with the temperature, as condensation effects are minimized in this case. This behavior has been modeled by Fouchet & Lellouch (2000) and introduced in the GCM by Montmessin et al. (2005). The positive correlation of D/H with the temperature and the water vapor content has been confirmed by the observations of Villanueva et al. (2015) and Krasnopolsky (2015).

Ground-based observations of Mars water are limited to times of adequate Doppler shift (generally greater than 10 km s^{-1}), but also permit much higher angular resolution and more frequent observations than are feasible with airborne observatories. On the other hand, they cannot be performed near opposition when the size of Mars is maximum, since the Doppler shift is then close to zero. The high-resolution cross-dispersed infrared spectrometers permit simultaneous detections and mapping of multiple species, including CO_2, H_2O, and HDO. In particular, the Echelon Cross Echelle Spectrograph (EXES) instrument aboard the Stratospheric Observatory for Infrared Astronomy (SOFIA) facility offers this possibility.

We used this instrument during its commissioning flight on April 8, 2014. A short spectral interval at 1383−1390 cm^{-1} (7.2 μm) was recorded over the Martian disk at high spectral resolution ($R = 6 \times 10^4$). The line depths of weak transitions of H_2O and HDO were divided by the line depth of a weak CO_2 transition in order to retrieve the H_2O and HDO mixing ratios over the Martian disk. Such a method was successfully used with the Texas Echelon Cross Echelle Spectrograph (TEXES) instrument, mounted at the InfraRed Telescope Facility (IRTF), to retrieve the H_2O_2 and HDO mixing ratios on Mars (Encrenaz et al. 2004, 2012, 2015). The D/H ratio is derived by ratioing the HDO and H_2O mixing ratios, taking into account that the D/H ratio is one-half of the HDO/H_2O value. In this specific case, the analysis can be done independently of the atmospheric structure retrieval. Indeed it has been shown (Encrenaz et al. 2015) that, for all thermal profiles expected during daily conditions (which corresponds to the EXES observations), the line depth ratios (or their equivalent widths, which give a similar result) provide a good estimate of the mixing ratio of the two species considered; thus, measuring the line depth ratio (or the equivalent width) HDO/H_2O leads to a good estimate of D/H. In our analysis, however, we also get estimates of the H_2O/CO_2 and HDO/CO_2 mixing ratios independently, in order to check the consistency of our results with respect to previous observations and models.

In this paper, we present the analysis of the EXES spectra of Mars. Section 2 describes the observations and the radiative transfer model used in our analysis. Section 3 describes the retrieval of the terrestrial atmospheric transmission associated with our observations, a key parameter in our retrieval of the mixing ratios of H_2O and HDO on Mars. The results are presented in Sect. 4. The validity of the linearity method is discussed in Sect. 5, and uncertainties are estimated in Sect. 6. Our results are discussed in Sect. 7 and compared with other observations and models.

2. Observations and modeling

2.1. Observations

EXES is an infrared imaging spectrometer derived from the TEXES instrument in operation at the NASA IRTF (Lacy et al. 2002). EXES operates between 4.5 and 28.3 μm (350−2220 cm^{-1}) in three different modes: high resolution (R = 50 000−100 000), medium resolution (R = 5000−20 000), and low resolution (R = 1000−3000). The instrument is equipped with a 1024 × 1024 Si:As detector array. The high-resolution mode is provided by a steeply blazed aluminum reflection grating used as an echelon, associated with an echelle grating to cross-disperse the spectrum (Richter et al. 2010).

We selected the 1383−1390 cm^{-1} interval because it contains both weak and strong transitions of H_2O, HDO, and CO_2. We used the instrument in the high-resolution mode. Observations

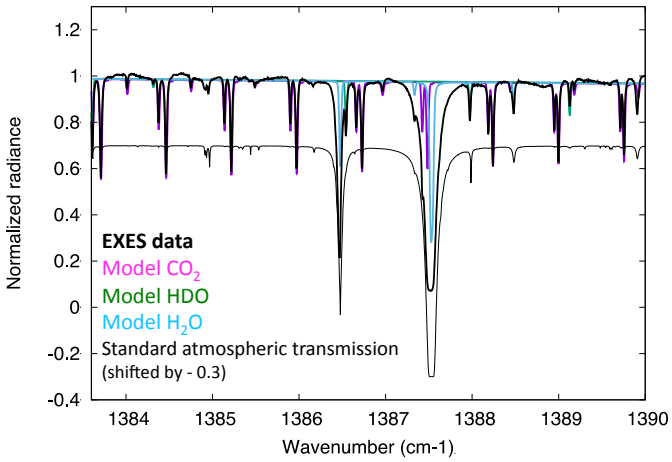

Fig. 1. Spectrum of Mars between 1383.5 and 1390.0 cm^{-1} (thick black line), integrated over the Martian disk, recorded with EXES (Ls = 113°, normalized radiance). Synthetic models of the Martian atmosphere: contributions from CO_2 (purple), H_2O (300 ppmv, blue), and HDO (467 ppbv, green). Thin black line (in absolute units shifted by −0.30): standard transmission from the terrestrial atmosphere, computed with the EXES model. The EXES spectrum shows an offset of 0.1 in the core of the strong water line at 1387.5 cm^{-1}, while the terrestrial atmospheric transmission is expected to be zero at this frequency.

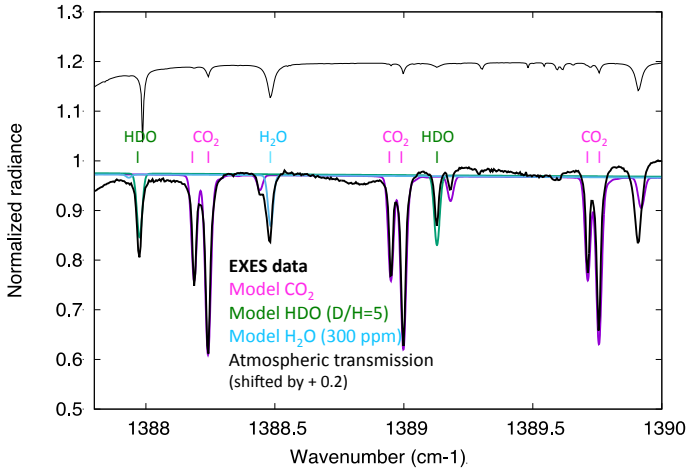

Fig. 2. Spectrum of Mars between 1387.8 and 1390.0 cm^{-1} (thick black line), integrated over the Martian disk, recorded with EXES (Ls = 113°, normalized radiance). Synthetic models of the Martian atmosphere: contributions from CO_2 (purple), H_2O (300 ppmv, blue), HDO (467 ppbv, green). The EXES spectrum and the models are enlargements of Fig. 1. Thin black line (in absolute units shifted by +0.20): standard transmission from the terrestrial atmosphere computed with the EXES model.

of Mars took place on April 8, 2014. SOFIA was flying at an altitude of 11.58 km. Mars was very close to opposition with a diameter of 15.07 arcsec, an illumination factor of 99.98%, and a Doppler velocity of −2.70 km s^{-1}. The season was just after northern summer solstice (Ls = 113°), corresponding to a maximum amount of water vapor in the northern region. The latitude and longitude of the disk center were 21.6 N and 205.0 E, respectively. The coordinates of the subsolar point were 23.0 N and 204.8 E. It must be noted that, unfortunately, the image quality of the SOFIA telescope is limited to about 3 arcsec. The image quality of 3 arcsec implies a longitudinal resolution of about 25 deg at the sub-Earth point. The slit was oriented at a position angle of 332 east of north and had a length of 14.2 arcsec (0.206 arcsec/pix) and a width of 1.44 arcsec. Because of the large size of the planet, we recorded two successive maps of opposite hemispheres of Mars that included significant overlap. The first scan was taken between 05:03:02 and 05:11:00 UTC with an initial offset from disk center of 8.16 arcsec W and 7.68 arcsec N. The scan was then performed taking 35 steps at 0.38 arcsec E and 0.55 arcsec S per step. The second scan was taken between 05:13:34 and 05:21:28 UTC with an initial offset from disk center of 3.12 arcsec W and 12.63 arcsec N and the same number and spacing for the steps as the first map. The final pixel size is 1.25 arcsec, i.e. more than twice smaller than the image quality of the SOFIA telescope. At 1387 cm^{-1}, the Doppler velocity of Mars corresponds to a Doppler shift of 0.0125 cm^{-1}, slightly smaller than the spectral resolution in the best case (0.0139 cm^{-1}).

Figure 1 shows the disk-integrated spectrum of Mars between 1383 and 1390 cm^{-1}. Synthetic spectra of Mars including CO_2, H_2O, and HDO are shown for comparison with a standard spectrum of the terrestrial atmospheric transmission, calculated for SOFIA observations. It can be seen that the spectrum of Mars is dominated by a regular series of CO_2 doublets. Two strong telluric absorption features due to H_2O (with a weak contribution of HDO) at 1386.5 cm^{-1} and 1387.5 cm^{-1} are superimposed on the Mars spectrum. Between 1387.8 and 1389.2 cm^{-1}, weak isolated lines of H_2O and HDO appear in the Mars spectrum (Fig. 2). In the center of the strong H_2O lines at 1386.5 and 1387.5 cm^{-1}, the EXES spectrum of Mars is completely dominated by the terrestrial absorption (Fig. 1). For this reason, we selected the 1387.8−1389.2 cm^{-1} for our analysis of the H_2O and HDO mixing ratios.

Figure 1 shows that the flux of the EXES spectrum in the core of the strong H_2O line at 1387.5 cm^{-1} is not equal to zero, while the terrestrial atmosphere is expected to be fully opaque at this frequency. This residual flux might be due to scattered light within the EXES instrument. In the present study, we remove it from the EXES spectra for comparison with the Martian synthetic spectra.

The retrieval of the H_2O and HDO mixing ratios on Mars critically depends upon the precise measurement of the terrestrial absorption contribution in the weak transitions used in our analysis. To obtain a precise measurement of the terrestrial contribution in these H_2O and HDO lines, we model the Earth's atmosphere and adjust the terrestrial temperature, pressure, and water content to obtain the best fit of the strong terrestrial absorption at 1386−1388 cm^{-1}. This method can be used because (1) H_2O is the main absorber in the telluric absorption; and (2) in this spectral range, the contribution of the Martian spectrum is very small as compared to the terrestrial absorption. For comparison with the EXES data, we use the integrated spectrum of Mars shown in Figs. 1 and 2 (after removal of the scattered component), in order to optimize its signal-to-noise ratio. The integrated spectrum can be used for this purpose because the terrestrial opacity is not expected to vary over the Martian disk.

2.2. Atmospheric modeling

To model the Martian synthetic spectrum, we use the radiative transfer code developed for our analysis of the TEXES data of Mars (Encrenaz et al. 2004, 2012, 2015). Spectroscopic data are extracted from the GEISA molecular database (Jacquinet-Husson et al. 2008). In the case of CO_2, the

Table 1. Spectroscopic parameters of the H_2O and HDO transitions used for the D/H retrieval.

Molecule	Wavenumber	*QN*(band)	*QN*(line)	*S*	*E*	Broad. coef.	*n*
	(cm^{-1})			($cm\ mol^{-1}$)	(cm^{-1})	($cm^{-1}\ atm^{-1}$)	
H_2O	1388.484	010 000	615 642	1.68×10^{-22}	757.8	0.105	0.46
HDO	1387.976	010 000	000 101	7.10×10^{-24}	15.5	0.206	0.69
HDO	1389.128	010 000	313 312	2.52×10^{-24}	116.5	0.192	0.67
CO_2	1388.187	100 01 000 01	R15E	4.09×10^{-26}	90.9	0.102	0.68
CO_2	1388.950	100 01 000 01	R16E	4.09×10^{-26}	103.0	0.101	0.68

self-broadening coefficients of the lines are given in the GEISA table. To account for their variation in temperature, we use the calculations of Rosenmann et al. (1988). In the case of H_2O and HDO, we use their broadening coefficients by CO_2 and their temperature dependences as described in Delaye et al. (1989). Table 1 shows the spectroscopic parameters of weak transitions of CO_2, H_2O and HDO in the 1387.8–1389.2 cm^{-1} range that are used in our calculations to map the species and to fit the spectra. As shown in Fig. 2, there is one available H_2O line at 1388.48 cm^{-1}, and there are two available HDO lines, at 1387.98 cm^{-1} and at 1389.13 cm^{-1}. At the positions of the two HDO lines, our inferred transmission function indicates comparable absorptions; however, the standard atmospheric transmission curve indicates a stronger absorption at 1387.98 cm^{-1} than at 1389.13 cm^{-1}, which indicates the possible presence of another contribution in the Earth atmosphere. Indeed, the EXES spectra show that the HDO line at 1387.98 cm^{-1} is systematically stronger than the other HDO line. For this reason, we adopt the HDO line at 1389.13 cm^{-1} in the following analysis. For CO_2, we use the weak transition at 1388.95 cm^{-1}, between the H_2O and HDO transitions selected for our analysis.

To correct the terrestrial absorption contribution in our spectra, we first consider the disk-integrated spectrum of Mars. For modeling this spectrum, we use the same temperature profile as Encrenaz et al. (2015) used for modeling the TEXES observations of March 1, 2014 (Ls = 96°); indeed, the GCM predictions at the disk center are very similar between March 1 and April 8. In this thermal profile, temperatures are 230 K, 170 K, and 145 K at altitude levels of 0 km, 20 km, and 40 km, respectively, with an isothermal profile above 40 km. We then adjust the surface pressure and temperature on Mars to obtain the best fit in the CO_2 lines of the EXES disk-integrated spectrum, because these lines are not affected by telluric contamination (Figs. 1 and 2). The derived disk-averaged surface pressure and surface brightness temperature on the surface of Mars are 6 mb and 255 K, respectively. It must be noted that these parameters, averaged over the Martian disk, are simply used to model the disk-integrated spectrum of Mars. The Martian atmospheric profile used in our modeling is not the only one that fits the CO_2 spectral lines but, as discussed in Encrenaz et al. (2015), the exact retrieval of the true Martian profile is not needed for our analysis, because it does not affect the line depth ratios as long as the CO_2 Martian lines are properly fitted. We also use the CO_2 lines to determine the spectral resolution of our data. Figure 3 shows different profiles (Gaussian and $sinc^2$) with FWHM values of 0.024 cm^{-1} and 0.028 cm^{-1}. We note that none of them is fully adapted to the EXES data because the EXES instrumental function exhibits broader wings. As a best fit, we use a FWHM of 0.024 cm^{-1}, corresponding to a resolving power of about 60 000 with a Gaussian profile (almost identical to the $sinc^2$ function).

In our nominal model of the disk-integrated spectrum of Mars (Figs. 1 and 2), we use, as a first try, mixing ratios of 300 ppmv for H_2O and 467 ppbv for HDO, corresponding to a Martian D/H of 5 (Encrenaz et al. 2015). Then, we divide the observed disk-integrated EXES spectrum by this model, and we adjust the parameters of the terrestrial absorption model to obtain the best fit in the regions of strong terrestrial absorption, where the contribution of Mars is almost negligible (see below, Sect. 3). Then, we multiply the inferred terrestrial transmission function with the Martian synthetic models for comparison with the EXES spectra and determination of the H_2O and HDO mixing ratios (see below).

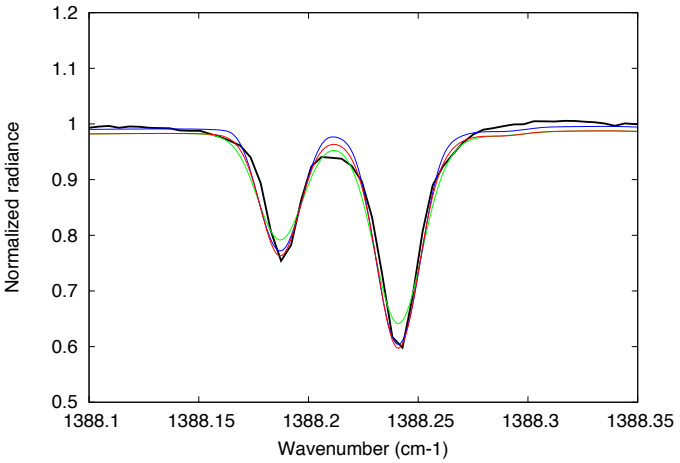

Fig. 3. Spectrum of Mars between 1388.10 and 1388.35 cm^{-1} (thick black line), integrated over the Martian disk, recorded with EXES (Ls = 113°, normalized radiance). Synthetic models of the Martian atmosphere with the CO_2 contribution for a FWHM value of 0.028 cm^{-1} with a Gaussian profile (green), a FWHM of 0.024 cm^{-1} with a Gaussian profile (red) and a FWHM of 0.024 cm^{-1} with a $sinc^2$ profile (blue). The two profiles with $FWHM = 0.024\ cm^{-1}$ are almost identical. The FWHM of 0.024 cm^{-1} with a Gaussian shape is adopted in our analysis.

3. Retrieval of the terrestrial atmospheric transmission

Two main factors determine the shape of the terrestrial atmospheric transmission in the H_2O and HDO absorptions: the pressure level above which the calculation is made, and the water vertical distribution above this level. We calculated a grid of spectra for different values of these parameters, and we compared the product of these curves with our nominal model of Mars to compare with the disk-integrated EXES spectrum of Mars. Calculations were done at high resolution (with a step of 0.001 cm^{-1}), taking the Doppler shift of Mars into account, and were convolved at the EXES spectral resolution for comparison with the EXES disk-integrated spectrum. The best fit transmission curve is shown in Fig. 4, compared with the standard transmission shown in Figs. 1 and 2. This transmission

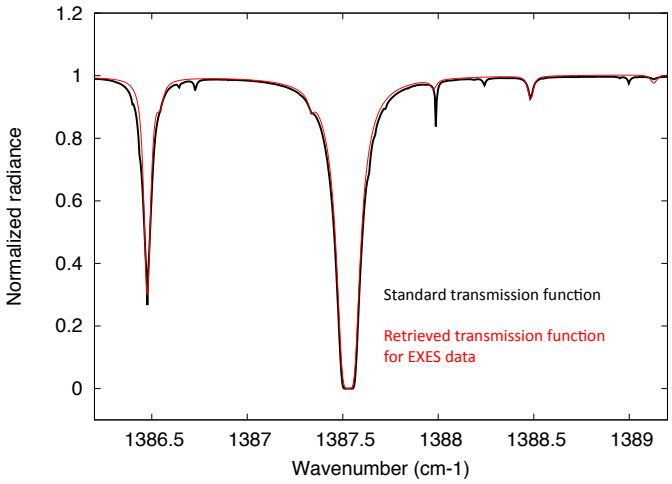

Fig. 4. Standard terrestrial atmospheric transmission (thick black line, also shown in Figs. 1 and 2) compared with our retrieved transmission function applicable for the EXES data of Mars. Our transmission curve was inferred from the best fit between the observed spectrum of Mars (after removal of the offset due to scattered light) and the product of the nominal synthetic model of Mars by the transmission function (see Fig. 5). The terrestrial atmospheric transmission is zero in the core of the strong water line at 1387.5 cm^{-1}.

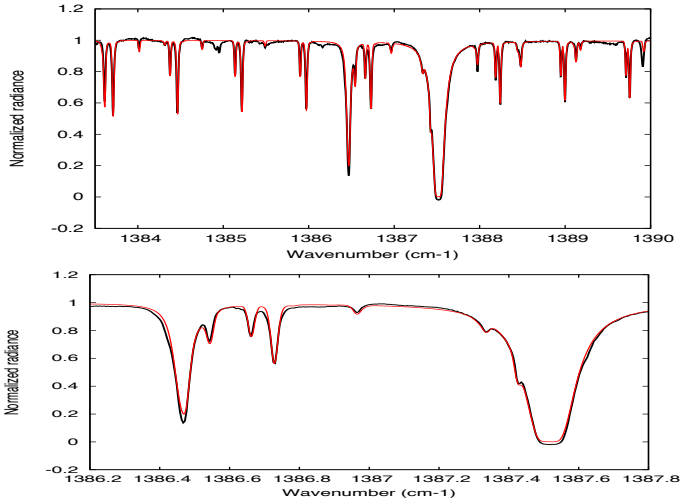

Fig. 5. Spectrum of Mars integrated over the Martian disk (thick black line), recorded with EXES on April 8, 2014 (Ls = 113°, normalized radiance). Red line: best-fit model of Mars multiplied by our inferred terrestrial atmospheric transmission function. *Top*: 1383.5–1390.1 cm^{-1}; *bottom*: 1386.2–1387.8 cm^{-1}. The radiance is zero at 1387.5 cm^{-1}, as expected from the opacity of the terrestrial atmosphere at this frequency.

curve corresponds to an altitude level of 11 km (consistent with the flight altitude of SOFIA of 11.6 km), a pressure of 0.17 bar, and a temperature of 185 K at this level. The terrestrial water mixing ratio ranges from 8×10^{-5} at the 11 km level to 2×10^{-5} at an altitude of 16 km and 5×10^{-6} at an altitude of 21 km.

Figure 5 shows the disk-integrated EXES spectrum of Mars compared with the product of our Martian model with the retrieved terrestrial atmospheric transmission. It can be seen that the agreement is quite satisfactory over the whole spectral range, in particular in the 1386.5 cm^{-1} and 1387.5 cm^{-1} water bands where the effect of the Martian spectrum is almost negligible. In what follows, we compare the EXES data with the Martian synthetic spectra multiplied by our retrieved transmission function,

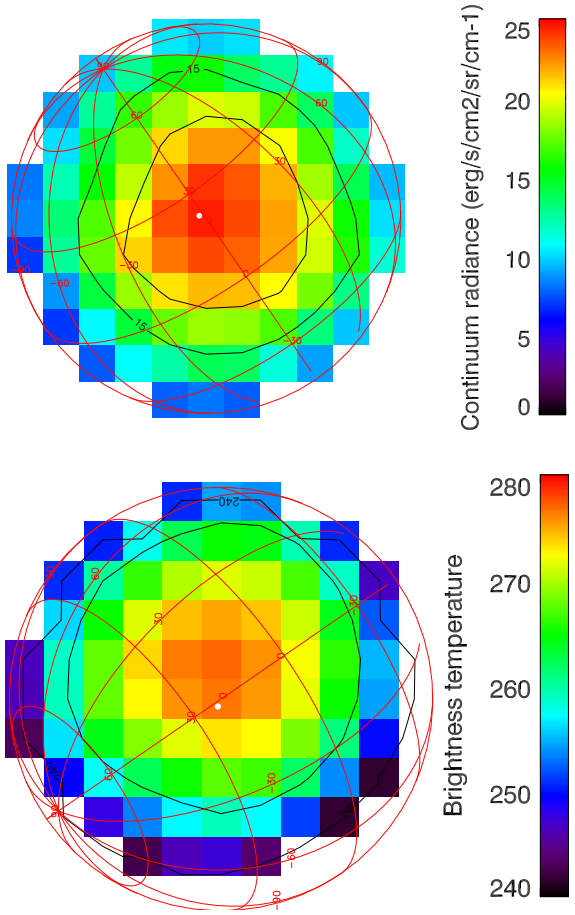

Fig. 6. Continuum maps of Mars with TEXES. *Top*: continuum radiance map of the Martian disk recorded at 1388.10 cm^{-1} (Ls = 113°) with EXES. *Bottom*: surface temperatures, assuming a maximum surface temperature of 280 K at the disk center, as predicted by the GCM. The absolute radiance scale is derived assuming that the brightness temperature is equal to the surface temperature, i.e.; that the surface emissivity is 1.0. The maps extend over 11 pixels in diameter, and the size of the pixel is 1.4 arcsec. The subsolar point is indicated by a white dot.

taking the Martian Doppler shift into account, and convolved with the EXES spectral resolution.

4. Mapping Mars

Figure 6 shows a map of the continuum radiance of Mars at 1388.60 cm^{-1} after removal of the scattered light. In the absence of absolute calibration available on the EXES instrument for our Mars data, we have retrieved a brightness temperature scale using the maximum surface temperature value expected at the disk center by the GCM (Forget et al. 1999) for the EXES observing conditions. We note that these temperature are actually upper limits to the actual brightness temperature, since our conversion assumes a surface emissivity of 1.0. We note that, in the case of our TEXES observations of Mars on March 1, 2014, an emissivity of 60% was inferred, corresponding to a drop of the brightness temperature by a few percent. The brightness temperature of 280 K is consistent with the GCM prediction (Forget et al. 1990), which indicates a maximum surface temperature of 290 K for our observing conditions. We did not consider the possible effects of dust aerosols on Mars. Since CO_2 has a different vertical distribution than H_2O and HDO, the presence of aerosols might affect the H_2O and HDO mixing ratios; however, because

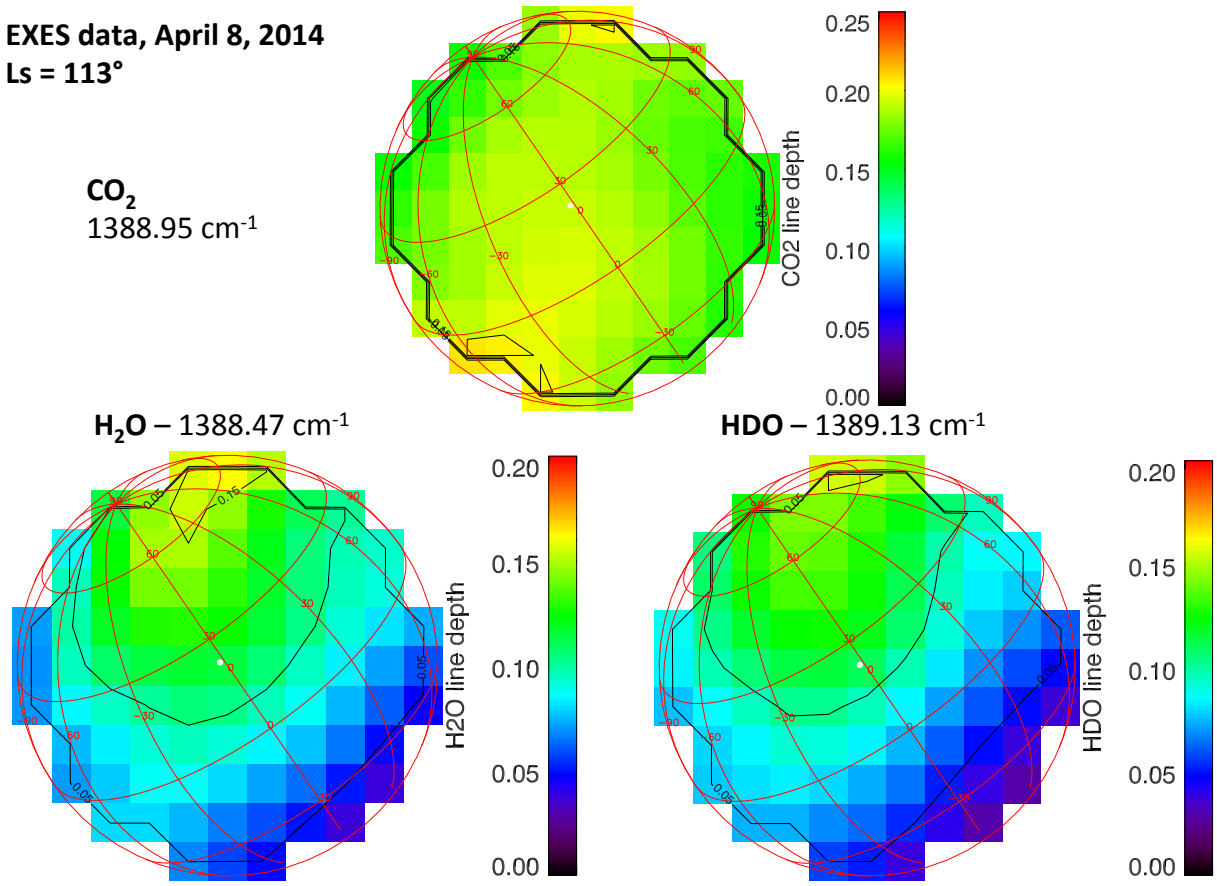

Fig. 7. Maps of the line depths for CO_2 at 1388.95 cm^{-1} (*top*), H_2O at 1388.47 cm^{-1} (*lower left*), and HDO at 1389.13 cm^{-1} (*lower right*), recorded with EXES (Ls = 113°). The subsolar point is indicated by a white dot.

the vertical distributions of H_2O and HDO are expected to be the same, the effect should be weak on the retrieval of the D/H map.

Figure 7 shows the maps of the line depths of CO_2 at 1388.95 cm^{-1}, H_2O at 1388.47 cm^{-1}, and HDO at 1389.13 cm^{-1}. It can be seen that the CO_2 line depth is always equal to 0.20 or higher, which illustrates that the temperature contrast between the surface and the atmosphere is sufficient for the linearity method described above to apply. This behavior is expected near opposition as the full dayside of Mars is observed. As expected, the H_2O and HDO line depth maps show similar behavior with a distinct enhancement around the north pole.

We have isolated three areas along the central meridian around the center and in the northern and southern regions, covering latitudes north of 45N and south of 30S, respectively. Each area covers 5×5 pixels on the planet, while the entire disk, with a diameter of 12 pixels, is covered by about 112 pixels. As in the case of the disk-integrated spectrum (Fig. 2), some fluctuations are present in the continuum, possibly owing to broad mineralogic features on the Mars surface or may have an instrumental origin. For comparison with the synthetic models, we removed these fluctuations by assuming, for each transition, a straight line between the continuum taken on each side of the transition. The result is shown in Figs. 8–11, which show the best fits obtained for the H_2O and HDO mixing ratios for the integrated disk, the disk center, and the northern and the southern regions, respectively. It can be seen that, in all cases, the two HDO lines cannot be fitted with a single HDO mixing ratio because the 1387.98 cm^{-1} line is systematically stronger. This suggests, as mentioned above, that some terrestrial contamination might still

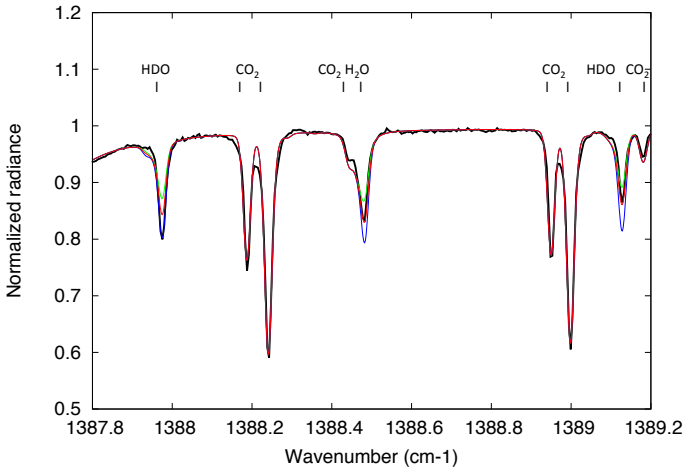

Fig. 8. EXES disk-integrated spectrum of Mars between 1387.9 and 1389.2 cm^{-1} (black line). Models: green: H_2O = 100 ppmv, HDO = 200 ppbv; red (best fit): H_2O = 220 ppmv, HDO = 300 ppbv; blue: H_2O = 380 ppmv, HDO = 475 ppbv. The surface pressure is 6 mb and the surface brightness temperature is 255 K. Synthetic spectra have been multiplied by the terrestrial absorption to fit the EXES data.

be present at this frequency, and we use the 1389.13 cm^{-1} transition for deriving the HDO mixing ratio.The following mixing ratios are inferred:

Disk-integrated spectrum: H_2O = 220 ppmv, HDO = 300 ppbv (D/H = 4.4 VSMOW);

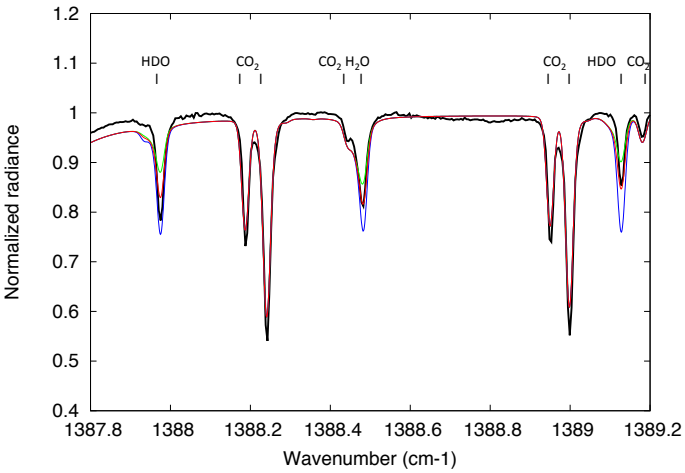

Fig. 9. EXES spectrum of Mars around the disk center between 1387.9 and 1389.2 cm^{-1} (black line). Models: green: H_2O = 150 ppmv, HDO = 250 ppbv; red (best fit): H_2O = 275 ppmv, HDO = 400 ppbv; blue: H_2O = 400 ppmv, HDO = 550 ppbv. The surface pressure is 7.5 mb and the surface brightness temperature is 280 K. The airmass is 1.0. Synthetic spectra have been multiplied by the terrestrial absorption to fit the EXES data.

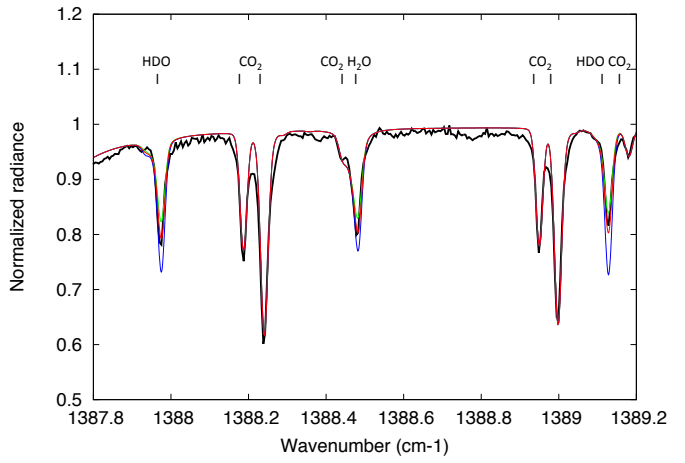

Fig. 10. EXES spectrum of Mars in the northern region between 1387.9 and 1389.2 cm^{-1}. Models: green: H_2O = 250 ppmv, HDO = 400 ppbv; red (best fit): H_2O = 375 ppmv, HDO = 550 ppbv; blue: H_2O = 600 ppmv, HDO = 950 ppbv. The surface pressure is 6 mb, and the surface brightness temperature is 240 K. The airmass is 1.75. Synthetic spectra have been multiplied by the terrestrial absorption to fit the EXES data.

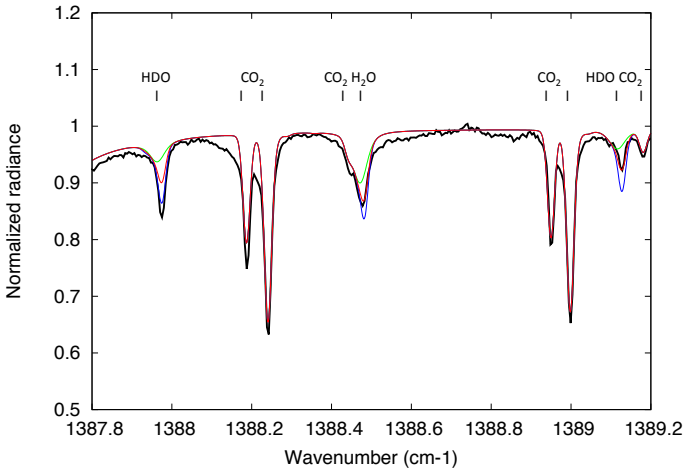

Fig. 11. EXES spectrum of Mars in the southern region between 1387.9 and 1389.2 cm^{-1} (black line). Models: green: H_2O = 0 ppmv, HDO = 0 ppbv; red (best fit): H_2O = 125 ppmv, HDO = 150 ppbv; blue: H_2O = 300 ppmv, HDO = 300 ppbv. The surface pressure is 5 mb and the surface brightness temperature is 235K. The airmass is 1.5. Synthetic spectra have been multiplied by the terrestrial absorption to fit the EXES data.

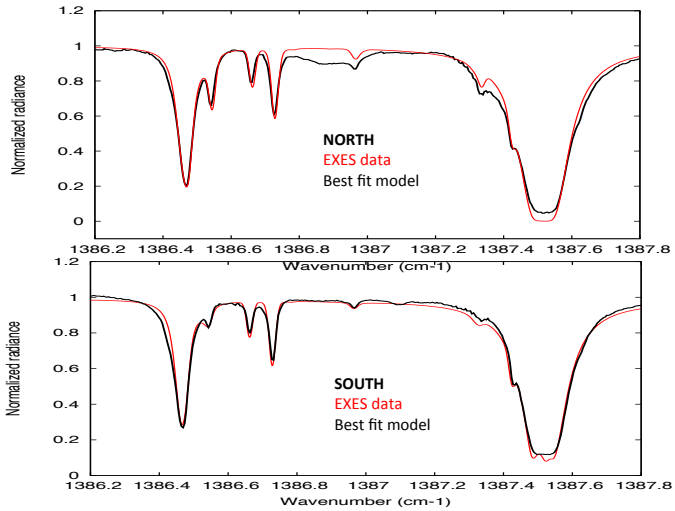

Fig. 12. Observed spectrum of Mars in the spectral range of maximum telluric absorption (1386.2–1387.8 cm^{-1}), compared with the best-fit model (red line, see Figs. 9 and 11). *Top*: northern region; *bottom*: southern region. The same plot is shown in Fig. 5 (*bottom*) for the observed disk-integrated spectrum.

Disk center: H_2O = 275 ppmv, HDO = 400 ppbv (D/H = 4.7 VSMOW);

Northern region: H_2O = 375 ppmv, HDO = 550 ppbv (D/H = (D/H = 4.7 VSMOW);

Southern region: H_2O = 125 ppmv, HDO = 150 ppbv (D/H = 3.9 VSMOW).

To check the consistency of our results in the northern and southern areas over the whole spectral range, we show the observed EXES spectra in Fig. 12 compared with the best-fit models multiplied by our transmission functions in the spectral range where the terrestrial absorption is maximum (1386–1388 cm^{-1}). These curves have to be compared with Fig. 5 for the full disk. It can be seen that the agreement is very satisfactory for the southern region, but not as good for the northern region. This may imply that the surface continuum shows variations in the northern hemisphere. Unfortunately, we have no way to account for these minor fluctuations. It can be noted that the HDO line appearing at 1386.55 cm^{-1} in the wing of the strong H_2O line centered at 1386.50 cm^{-1} is well fit in both regions.

Figure 13 shows the maps of the H_2O and HDO mixing ratios relative to CO_2, inferred from the line depth ratios of the 1388.47 cm^{-1} H_2O line and the 1389.13 cm $^{-1}$ HDO line, divided by the 1388.95 cm^{-1} CO_2 line. The linearity relationship between the line depth ratios (ldr) and the volume mixing ratios (vmr) are derived from the best-fit model for the disk center and are defined as follows:

$$\mathrm{vmr}(H_2O)(\mathrm{ppmv}) = 509.2 \times \mathrm{ldr}(H_2O/CO_2)$$
$$\mathrm{vmr}(\mathrm{HDO})(\mathrm{ppbv}) = 723.7 \times \mathrm{ldr}(\mathrm{HDO}/CO_2).$$

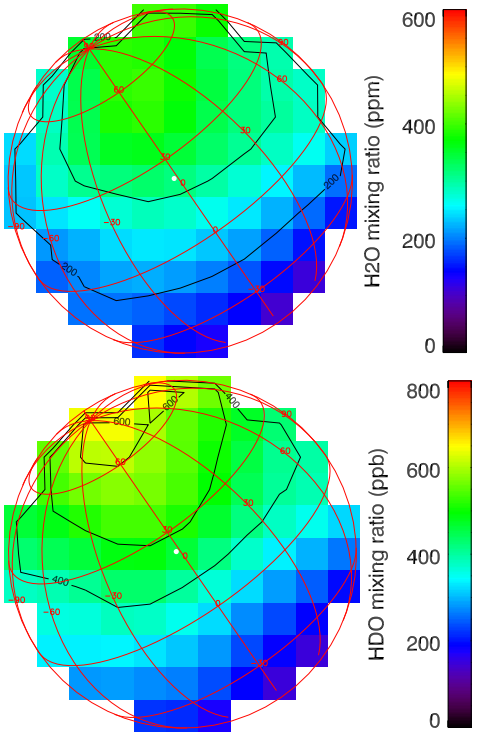

Fig. 13. *Top*: map of the H_2O volume mixing ratio (in ppmv) retrieved from the EXES data recorded on April 8, 2014 (Ls = 113°), converted from the H_2O/CO_2 line depth ratio (see text). *Bottom*: map of the HDO volume mixing ratio (in ppbv) retrieved from the same data, converted from the HDO/CO_2 line depth ratio. The subsolar point is indicated by a white dot.

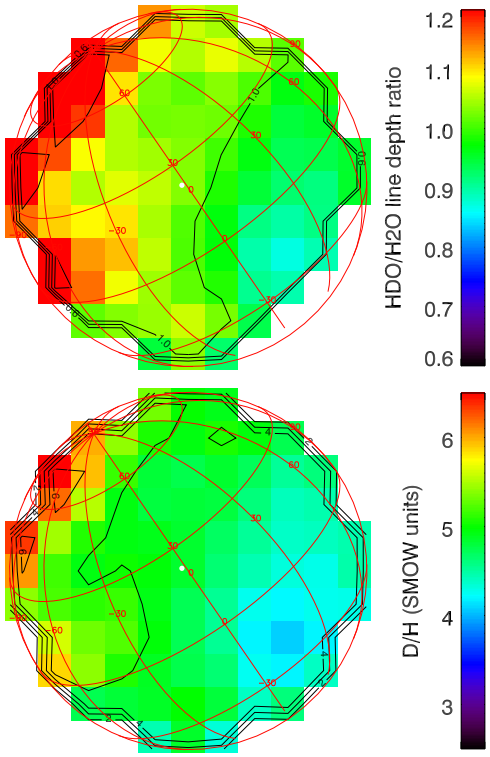

Fig. 14. *Top*: map of the HDO/H_2O line depth ratio, retrieved from the EXES data recorded on April 8, 2014 (Ls = 113°). *Bottom*: map of the D/H mixing ratio (in VSMOW units) converted from the HDO/H_2O line depth ratio (see text). The subsolar point is indicated by a white dot.

The D/H ratio can be inferred from the line depth ratio of the HDO and H_2O lines. This method has the advantage of removing the uncertainties associated with the thermal structure and the geometry as much as possible and of minimizing the uncertainties associated with the terrestrial atmospheric transmission. The validity of the linearity method is discussed below. We derive D/H (VSMOW units) = 4.60 × ldr (HDO/H_2O). Figure 14 shows the map of the D/H ratio on Mars in line depth ratio units and in VSMOW units.

5. Linearity of the mixing ratios with the line depth ratios

We have shown in our previous analyses (Encrenaz et al. 2008, 2015) that the mixing ratio of two atmospheric species can be directly inferred from the ratio of their line depths provided that the lines are weak with line depths less than about 10% to 15%. This assumption also requires that the two species are homogeneously mixed and that the temperature contrast between the surface and the atmosphere is sufficient. Near terminator, at night, before dawn, or after sunset, these conditions may not be filled (Encrenaz et al. 2015). In the present case, observations are made near opposition, and the full dayside of Mars is observed, so this condition is fulfilled.

However, a departure from linearity is expected to occur because the CO_2 line depth is about 0.20–0.25, so larger than in our TEXES analysis. This uncertainty should be reduced on the measurement of the D/H ratio, as D/H is directly retrieved from the ratio of the HDO and H_2O line depths, which both have a line depth between 5% and 15%. Still, some error may be introduced because the individual lines are not optically thin. In addition, the quantum numbers of the H_2O and HDO lines used for the map retrieval are very different, as shown in Table 1. This difference may introduce systematic uncertainties related to vertical profiles of temperature and abundances. However, as pointed out above, both H_2O and HDO are expected to have similar distribution: Near northern summer solstice (Ls = 113°), the atmosphere is cold and the two species are confined in the lower troposphere, so this effect is expected to be minor.

Using the thermal profile and the atmospheric parameters corresponding to the disk center, we determined the HDO/H_2O line depth ratio for a D/H ratio of 4.7 VSMOW (corresponding to the best fit at the center) and for different values of the H_2O volume mixing ratio. Calculations show that a departure from linearity of 10% is observed for H_2O mixing ratios of half and twice the best fit value of 275 ppmv, respectively. The linearity method is thus expected to undersestimate the D/H value in the southern hemisphere and to overestimate in the northern hemisphere by a factor of 10%.

6. Uncertainty analysis

We first estimate the instrumental noise in the EXES data. Figure 15 shows an enlargement of the disk-integrated spectrum of Mars in the continuum region around 1388.8 cm^{-1}. It can be seen that the peak-to-peak (3σ) noise in the disk-integrated spectrum is less than 1%. Since the full disk is covered by 112 pixels, the 1σ noise per pixel is less than 3%. This noise is much lower than the uncertainty induced by (1) the uncertainty in the instrumental function (see Fig. 3) and (2) the uncertainty associated with the telluric atmospheric transmission.

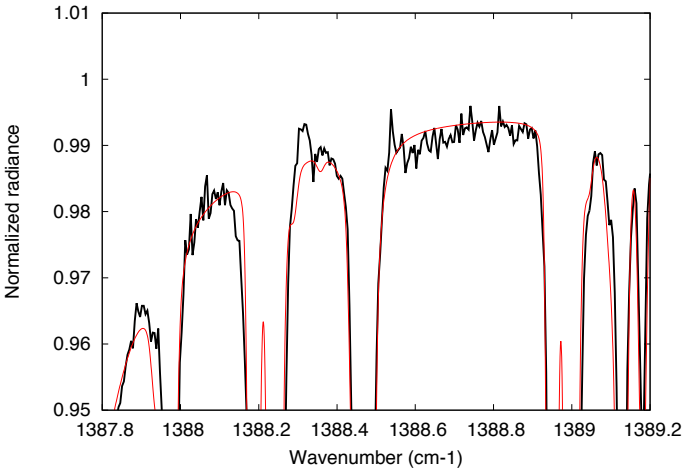

Fig. 15. Spectrum of Mars between 1387.8 and 1389.2 cm^{-1} (thick black line), integrated over the Martian disk, recorded with EXES (Ls = 113°, normalized radiance). Red line: synthetic spectrum of the Martian atmosphere corresponding to the best fit (Fig. 8): H_2O = 220 ppmv, HDO = 300 ppbv.

In the first case, the error is maximum in the retrieval of the H_2O line depth at 1388.47 cm^{-1} because of the limited quality of the fit of the weak neighboring CO_2 line at 1388.44 cm^{-1}. Owing to the uncertainty in the continuum level between the CO_2 and H_2O lines at 1388.455 cm^{-1}, we estimate that the absolute error on the H_2O line depth is about 20% for the disk-integrated spectrum, 15% for the center and the northern region, and 30% for the southern region. The measurement of the HDO line depth at 1389.13 cm^{-1} is not affected by this effect.

To estimate the uncertainty associated with the retrieval of the terrestrial atmospheric transmission, we took two extreme cases for the terrestrial contribution in the H_2O and HDO line depths. With the retrieved atmospheric transmission curve used in this study, the terrestrial contribution (in depth) is 0.065 for the H_2O line at 1388.47 cm^{-1} and 0.026 for the HDO line at 1389.13 cm^{-1}, which is 0.4 times its value for H_2O (see Fig. 4). The total depth of the H_2O line (including the terrestrial contribution) in the EXES spectrum of the southern region is 0.10. We estimated that the terrestrial contribution in this line cannot be more than 0.075 in order to avoid negligible (and unreasonably low) values of the Martian H_2O in this region. We scaled the terrestrial contribution HDO accordingly at 0.030. For the lower limits of terrestrial absorption, we assumed 0.055 for the H_2O line and 0.022 for the HDO lines.

The uncertainties on the H_2O and HDO mixing ratios on Mars can be estimated as follows. For the disk-integrated spectrum of Mars, the H_2O nominal line depth (without the terrestrial contribution) is about 0.10 (Figs. 7 and 8). In the case of H_2O, using the two extreme values of the terrestrial contribution leads to extreme line depths ranging from 0.09 to 0.11, corresponding to an uncertainty of 10%. The associated uncertainty is 7% for the northern region and 20% for the southern region. These uncertainties have to be combined quadratically with the error associated with the poor quality of the fit as discussed above. The resulting uncertainties on the H_2O mixing ratio are 22% for the disk-integrated value, 17% for the center and the northern region, and 36% for the southern region.

In the case of HDO, the line depth in the disk-integrated spectrum (without the terrestrial contribution) is about 0.10. It becomes 0.096 if the terrestrial absorption is maximum and 0.104 in the opposite case. The associated uncertainty is then 4%. It becomes 3% at the center and in the northern region and 10% in the southern region.

Because the terrestrial absorption contribution has no effect on the CO_2 line depth, its uncertainty is minor compared with the H_2O and HDO line depths. The final results are thus the following:

Disk-integrated spectrum: H_2O = 220+/−48 ppmv, HDO = 300+/−12 ppbv;

Disk center: H_2O = 275+/−47 ppmv, HDO = 400+/−12 ppbv;

Northern region: H_2O = 375+/−64 ppmv, HDO = 550+/−17 ppbv;

Southern region: H_2O = 125+/−45 ppmv, HDO = 150+/−15 ppbv.

It should be noted that these error bars are systematic. The relative error bars on the H_2O and HDO maps (Figs. 12) are much lower and only due to the signal-to-noise ratio of the EXES spectrum in one pixel. As discussed above, the 1σ associated uncertainty is 3%.

The absolute uncertainty on the D/H ratio is obtained by associating, on one hand, the maximum values of H_2O and HDO mixing ratios and, on the other, their minimum values. The result is the following:

Disk-integrated spectrum: D/H = 4.4 (+1.0, −0.6) VSMOW;

Disk center: D/H = 4.7 (+0.8, −0.6) VSMOW;

Northern region: D/H = 4.7 (+0.8, −0.6) VSMOW;

Southern region: D/H = 3.9 (+ 1.5, −0.8) VSMOW.

The relative uncertainty on the D/H variations shown in the D/H map (Fig. 13) is the quadratic combination of the errors on the H_2O and HDO line depths. The 1σ uncertainty is thus 4.2%.

7. Discussion

Our observation of Mars with EXES leads to a disk-integrated value of 4.4 (+1.0, −0.6) times the VSMOW value. This value tends to be slightly lower than most of the previous disk-integrated determinations, although still consistent with most of them taking the error bars into account (Owen et al. 1988; Krasnopolsky et al. 1997). Part of the difference can be explained by the fact that, at the time of our observations, the Tharsis plateau was in the field of view; indeed, lower D/H values are expected in high-altitude regions where the water vapor content is lower. Figure 16 show a closer comparison of our data with the maps obtained by Villanueva et al. (2015) for Ls = 80 and 83°. The D/H ratio above the Tharsis region is clearly depleted in our map, which is in good agreement with the data of Villanueva et al. (2015). The poor spatial resolution of our map is a consequence of the poor image quality of the SOFIA telescope, which is limited to about 3 arcsec, corresponding to two pixels on our map. We thus confirm the low D/H values for high-altitude regions of Mars. However, at latitudes higher than the Tharsis plateau, our D/H is uniformly close to 5 VSMOW while, in the map shown by Villanueva et al. (2015), it reaches about seven times the VSMOW at 60N north of Olympus Mons, over a region that is larger than our spatial resolution (Fig. 16). Independently of its limited spatial resolution, the EXES map seems to show less variability than the data of Villanueva et al. (2015).

Our D/H measurement can also be compared with Krasnopolsky's result for the same season. For Ls = 110°, Krasnopolsky's value of D/H is about four VSMOW in the northern hemisphere, in agreement with our result. We note that the longitude range for Krasnopolsky's measurements (Central Meridian at 253 E) was different from the conditions of the

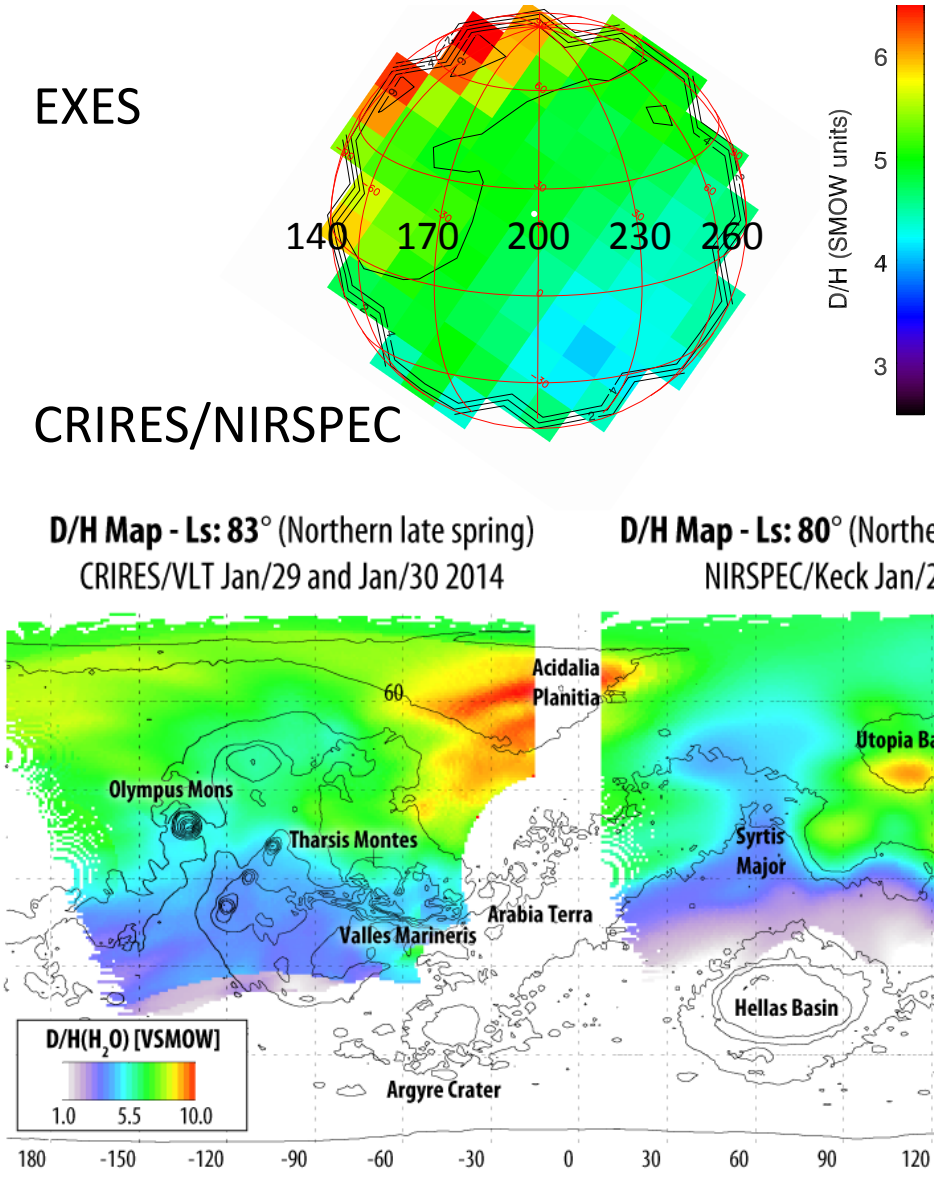

Fig. 16. *Top*: map of the D/H ratio in VSMOW units retrieved from the EXES data recorded on April 8, 2014 (Ls = 113°, same as Fig. 13, *bottom*). *Bottom*: map of the D/H mixing ratio (in VSMOW units) retrieved by Villanueva et al. (2015) in January 2014 for Ls = 80 deg and 83 deg. The left map of Villanueva et al. (2015) matches the longitude range covered by the EXES observations.

EXES observations (Central Meridian at 205 E). The mean global D/H reported by Krasnopolsky (2015), integrated over the disk and over time, is 4.6+/−0.7 VSMOW, in good agreement also with the EXES result.

The EXES maps of HDO and H_2O can be compared with the GCM predictions and with previous observations. In the case of the HDO map, a comparison can be made with the results recorded by the TEXES imaging spectrometer on the IRTF on March 1, 2014 (Encrenaz et al. 2015) for Ls = 96°. The map of the HDO mixing ratio was obtained from the line depth ratio of a weak HDO transition at 1237.08 cm^{-1} (8.08 μm) divided by a weak nearby CO_2 line at 1241.58 cm^{-1} (8.05 μm). Figure 17 shows a comparison of the TEXES and EXES maps, separated in time by five weeks and in areocentric longitude by 17°. The overall agreement is satisfactory, both for the HDO mixing ratio and its global distribution over the disk. Figure 17 also shows a comparison of the two HDO maps with the predictions of the GCM (Montmessin et al. 2005). For both the EXES and TEXES data, the agreement is satisfactory except at the north pole where the GCM prediction is higher than the observed one (by both TEXES and EXES) by a factor of 1.5 to 2 over a region as large as the EXES spatial resolution.

Our H_2O map can also be compared with previous observations. The EXES map of H_2O is consistent with the map of Villanueva et al. (2015) for Ls = 80−83°. For Ls = 113°, the TES data aboard Mars Global Surveyor (Smith 2004) indicate an H_2O column density ranging from 4 pr-μm at 30S latitude to 12 pr-μm at the equator and 40 pr-μm at 60N latitude. In our model, these numbers correspond to 77 ppmv, 204 ppmv, and 680 ppmv at 30S, 0, and 70N latitudes, respectively. At 30S and 0 latitude, these numbers are consistent with our results, taking the error bars into account. At high northern latitudes, the TES value is higher than our result by about 30%. The same comment applies to the comparison of our EXES map with the predictions of the GCM (Forget et al. 1999, Fig. 18). The EXES values are consistent with the GCM values, except in

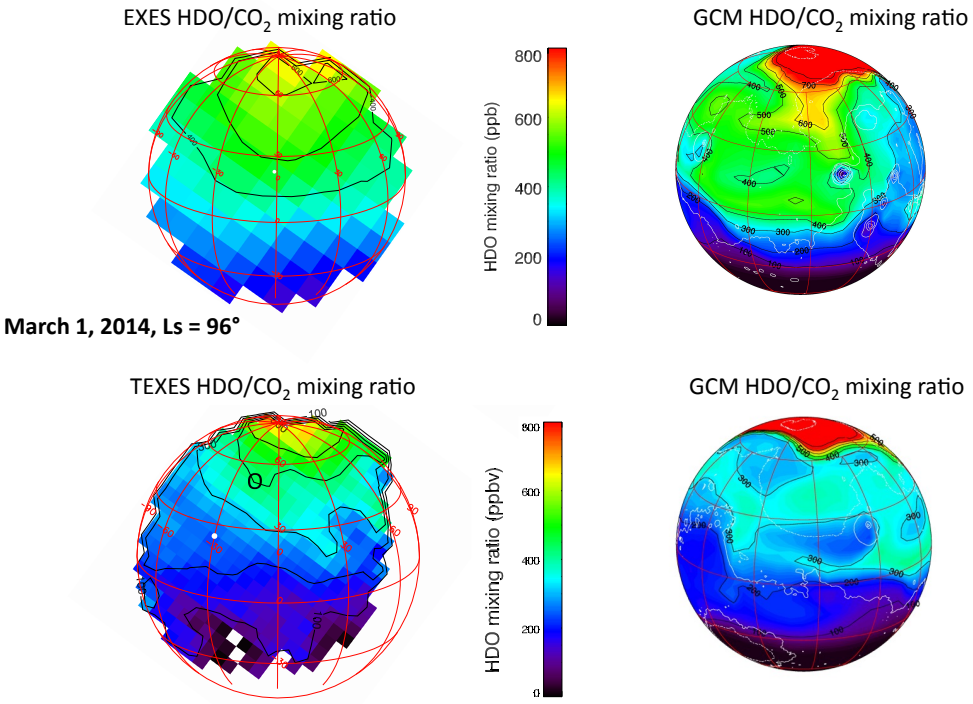

Fig. 17. *Top left*: map of the HDO/CO_2 volume mixing ratio, retrieved from the EXES data recorded on April 8, 2014 (Ls = 113°). *Top right*: GCM prediction for the same observing conditions (after Montmessin et al. 2005). *Bottom left*: map of the HDO/CO_2 volume mixing ratio retrieved from the TEXES data on March 1, 2014 (Ls = 96°). *Bottom right*: GCM prediction for the same observing conditions (Encrenaz et al. 2015).

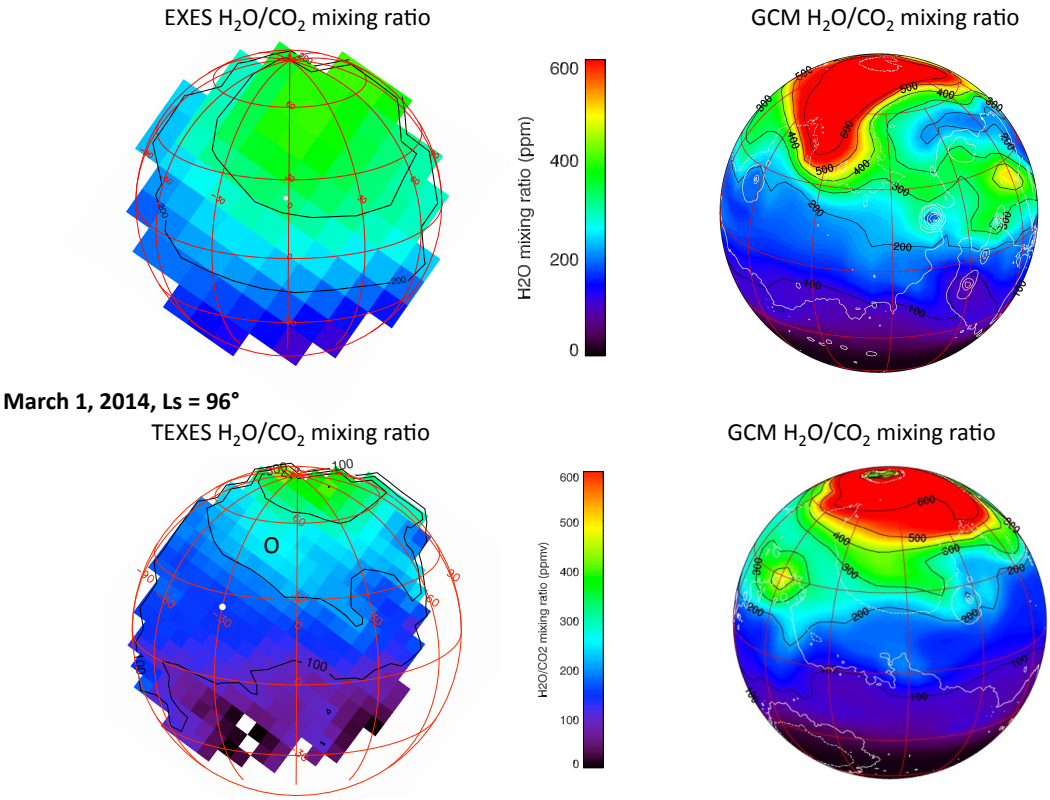

Fig. 18. *Top left*: map of the H_2O/CO_2 volume mixing ratio, retrieved from the EXES data recorded on April 8, 2014 (Ls = 113°). *Top right*: GCM predictions for the same observing conditions. *Bottom left*: map of the H_2O/CO_2 volume mixing ratio retrieved from the TEXES data on March 1, 2014 (Ls = 96°, *left*), assuming a uniform D/H ratio of 5 VSMOW. *Bottom right*: GCM prediction for the same observing conditions (Encrenaz et al. 2015).

the northern region where they are significantly weaker. We note that the TEXES map of H_2O was inferred using a D/H mean value of 5 VSMOW, so slightly higher than the EXES value, which explains the lower values of the TEXES H_2O map with respect to the EXES map (Fig. 18).

The H_2O latitudinal distribution observed by EXES can also be compared with the result reported by Krasnopolsky (2015) for Ls = 110°. Krasnopolsky (2015) derives a H_2O column density of about 15 pr-μm and 35 pr-μm at latitudes of 20 N and 80 N, respectively. Using our model, these numbers translate into 255 ppmv and 600 ppmv, which is consistent with the EXES result. The departure from the GCM in the water vapor map at high northern latitudes is thus observed by the different ground-based observations, which might suggest that some adjustment is required in the GCM to fit the data better around the north pole.

From the water vapor spatial distribution shown in Figs. 13 and 17, it is possible to estimate the D/H map expected if the VPIE is the main mechanism responsible for fractionation. Following Fouchet & Lellouch (2000), we consider an open cloud system, where the solid phase condenses in isotopic equilibrium with the water phase and leaves the cloud by precipitation immediately after its formation (Dansgaard 1964). In this case we expect

$$1 + \delta = [n_V / n_{V0}] \exp(\alpha - 1),$$

where δ is the isotopic departure with respect to the reference D/H value, n_{V0} is the reference (maximum) water vapor content, and α the fractionation coefficient, which is the ratio of the D/H ratio in the condensed phase to the ratio in the vapor phase (Merlivat & Nief 1967). Following Fouchet & Lellouch (2000), we adopt $\alpha = 1.24$, corresponding to a temperature of 230 K. We calculate the expected D/H value in the southern region, using $n_V = 125$ ppmv (as derived from the EXES data), and as reference values, the water vapor volume mixing ratio and the D/H value inferred from EXES in the northern region ($n_{V0} = 375$ ppmv, D/H = 4.7 × VSMOW). Using these parameters, we infer, for the southern region, a D/H ratio of 3.6 × VSMOW, in good agreement with the EXES value. We conclude that the EXES results are fully consistent with the VPIE mechanism being responsible for the deuterium fractionation on Mars. We also note that the above calculation gives an upper limit of the deuterium fractionation expected from the VPIE, considering that the open cloud assumption is an extreme case (because it assumes that the solid phase leaves the cloud immediately after its formation). Thus, assuming the VPIE process, we do not expect stronger D/H variations than observed in our map (Fig. 13).

Our analysis confirms the expected behavior of the D/H ratio as a function of altitude and as a function of the H_2O abundance, previously illustrated by Villanueva et al. (2015) and Krasnopolsky (2015). We cannot confirm the high global value of the D/H enrichment over the seasonal cycle inferred by the authors. Indeed, our observations covered a longitude range where low values of D/H were expected. Other observations with EXES aboard SOFIA will be needed for different seasons of the Martian cycle to infer a global value of the D/H ratio, averaged over the whole seasonal cycle.

Acknowledgements. This article is based on observations made with the NASA/DLR Stratospheric Observatory for Infrared Astronomy (SOFIA). SOFIA is jointly operated by the Universities Space Research Association, Inc. (USRA), under NASA contract NAS2-97001, and the Deutsches SOFIA Institut (DSI) under DLR contract 50 OK 0901 to the University of Stuttgart. Financial support for this work was provided by NASA. We wish to thank the SOFIA and EXES staff for the support of EXES observations. We are grateful to M. J. Mumma for helpful comments regarding this paper. T.K.G. acknowledges support of NASA Grant NNX14AG34G. T.E. and B.B. acknowledge support from CNRS and Programme National de Planétologie. T.F. acknowledges support from UPMC. T.E. acknowledges support from Jet Propulsion Laboratory as a Distinguished Visiting Scientist.

References

Bertaux, J.-L., & Montmessin, F. 2001, J. Geophys. Res., 106, 32879
Bjoraker, G. L., Mumma, M. J., & Larson, H. P. 1989, BAAS, 21, 991
Boctor, N. Z., Alexander, C. M. O. D., Wang, J., & Hauri, E. 2003, Geochim. Cosmochim. Acta, 67, 3971
Carr, M. H. 1986, Icarus, 68, 187
Carr, M. H. 1996, Water on Mars (Oxford: Oxford University Press)
Carr, M. 1990, Icarus, 87, 210
Dansgaard, W. 1964, Tellus, 16, 436
Delaye, C., Hartmann, J. M., & Taine 1989, J. Appl. Opt., 28, 5085
Encrenaz, T., Lellouch, E., Rosenqvist, J., et al. 1991, Ann. Geophys., 9, 797
Encrenaz, T., Lellouch, E., Paubert, G., et al. 2001, Plan. Space Sci., 49, 731
Encrenaz, T., Bézard, B., Greathouse, T. K., et al. 2004, Icarus, 170, 424
Encrenaz, T., Greathouse, T. K., Richter, M. J., et al. 2008, Icarus, 195, 547
Encrenaz, T., Greathouse, T. K., Lefèvre, F., et al. 2012, Plan. Space Sci., 68, 3
Encrenaz, T., Greathouse, T. K., Lefèvre, F., et al. 2015, A&A, 578, A127
Forget, F., Hourdin, F., Fournier, R., et al. 1999, J. Geophys. Res., 104, 24155
Fouchet, T., & Lellouch, E. 2000, Icarus, 144, 114
Jacquinet-Husson, N., Scott, N., Chedin, A., et al. 2008, J. Quant. Spectr. Rad. Transf., 109, 1043
Jakosky, B. M. 1990, J. Geophys. Res., 95, 1475
Krasnopolsky, V. A. 2002, J. Geophys. Res., 107, 5128
Krasnopolsky, V. A. 2015, Icarus, 257, 377
Krasnopolsky, V. A., & Feldman, P. D. 2001, Science, 294, 1914
Krasnopolsky, V. A., Bjoraker, G. L., Mumma, M. J., & Jenning, D. E. 1997, J. Geophys. Res., 102, 6525
Krasnopolsky, V. A., Mumma, M. J., & Gladstone, R. G. 1998, Science, 280, 1576
Lacy, J. H., Richter, M. J., Greathouse, T. K., et al. 2002, PASP, 114, 153
Lasue, J., Mangold, N., Hauber, E., et al. 2013, Space Sci. Rev., 174, 155
Mahaffy, P. R., Webster, C. R., & Stern, J. C. 2015, Science, 347, 412
Merlivat, L., & Nief, G. 1967, Tellus, 19, 122
Montmessin, F., Fouchet, T., & Forget, F. 2005, J. Geophys. Res., 110, E03006
Mouginot, J., Pommerol, A., Beck, P., et al. 2012, Geophys. Res. Let., 39, L02202
Mumma, M. J., Novak, R. E., Disanti, M. A., et al. 2003, Sixth International Conference on Mars, Pasadena, CA, July 2003, abstract #3186
Owen, T. 1992, The composition and early history of the atmosphere of Mars. In Mars, eds. H. H. Kieffer, et al. (Tucson: University of Arizona Press)
Owen, T., Maillard, J.-P., de Bergh, C., & Lutz, B. L. 1988, Science, 240, 1767
Plaut, J. J., Picardi, G., Safaeinili, A., et al. 2007, Science, 316, 92
Richter, M. J., Ennico, K. A., Mc Kelvey, M. E., & Seifhart, A. 2010, Proc. SPIE7735 "Ground-based and Airborne Instrumentation for Astronomy – III", eds. I. S. McLean, S. Ramsay, & H. Takami, San Diego, Ca, USA, June 2010
Rosenmann, L., Hartmann, J. M., Perrin, M. Y., & Taine 1988, J. Appl. Opt., 27, 3902
Smith, M. D. 2004, Icarus, 167, 148
Usui, T., Alexander, C. M. O., Wang, J., Simon, J. I., & Jones, J. H. 2012, 43rd Lunar and Planetary Science Conference, 43, 1341
Villanueva, G. L., Mumma, M. J., Novak, R. E., et al. 2015, Science, 348, 218
Wordsworth, R. D., Kerber, L., Pierrehumbert, R. T., et al. 2015, J. Geophys. Res. DOI: 10.1002/2015JE004787
Zahnle, K., Kasting, J. F., & Pollack, J. B. 1990, Icarus, 84, 502
Zuber, M. T., Smith, D. E., Solomon, S. C., et al. 1998, Science, 282, 2053